Validity of a closed-form diffusion solution in P_1 approximation for reflectance imaging with an oblique beam of arbitrary profile

Jun Q. Lu and Cheng Chen
Department of Physics, East Carolina University, Greenville, North Carolina 27858

David W. Pravica
Department of Mathematics, East Carolina University, Greenville, North Carolina 27858

R. Scott Brock and Xin-Hua Hu[a)]
Department of Physics, East Carolina University, Greenville, North Carolina 27858

(Received 28 April 2008; revised 16 July 2008; accepted for publication 17 July 2008; published 8 August 2008)

Determination of optical parameters of turbid media from reflectance image data is an important class of inverse problems due to its potential for noninvasive characterization of materials and biological tissues, which demands rapid modeling tools to generate calculated images. We treat the problem of reflectance imaging with homogeneous semi-infinite turbid media as a boundary-value problem of diffusion type in the P_1 approximation to the radiative transfer equation. A closed-form solution has been obtained for an oblique incident beam of arbitrary profile and its accuracy has been examined against a Monte Carlo method and measured data. We find that the diffusion solution provides a sufficiently accurate tool to rapidly calculate reflectance images for samples of large or moderate scattering albedo illuminated by a beam of arbitrary profile as long as the anisotropy factor remains less than 0.7 and single scattering albedo larger than 0.8. The closed-form solution can thus be used as a part of a forward modeling toolbox to determine optical parameters from reflectance image data in combination with other method such as the Monte Carlo simulation. © *2008 American Association of Physicists in Medicine*. [DOI: 10.1118/1.2968332]

Key words: reflectance imaging, diffusion approximation, turbid medium

I. INTRODUCTION

Continuous-wave reflectance imaging with a full-field illumination provides a simple and noncontact means to interrogate optically thick materials. As the imagers with high dynamic range and spatial resolution have become readily available at low cost, reflectance imaging of scattered and fluorescence light signals in the visible and near-infrared regions has attracted active research efforts for clinical and other applications.[1–3] Determination of the optical parameters related to light absorption and scattering from the reflectance image data is highly desired in these cases because of the correlation between these parameters and the *in vivo* physiological and pathological information of tissues.[4,5] The strong volumetric light scattering in most human and animal tissues, however, presents a major challenge to accurately determine these parameters from the measured image data. An essential part of solving the above inverse problems is to develop rapid and yet sufficiently accurate tools for modeling tissue optics. At the macroscopic scales of 0.1 mm or larger, much greater than wavelengths, light interaction with turbid tissues can be modeled accurately as a boundary-value problem characterized by a radiative transfer equation (RTE) and appropriate boundary conditions. For problems with realistic boundaries, including incident beams of arbitrary profiles, and medium heterogeneity, numerical approaches have to be resorted such as the finite-difference discrete-ordinate method[6] and the Monte Carlo (MC) method.[7]

Instead of solving the RTE based boundary-value problems directly, one can obtain light distributions with a MC method by sampling a large number of photons undergoing stochastic processes of absorption and scattering. These processes are characterized by the probability distribution functions based on the RT theory and therefore the obtained results provide equivalent solutions. The MC method has been used extensively to solve tissue optics problems with homogeneous and heterogeneous distribution of optical parameters for its algorithmic simplicity and subsequent versatility.[8–13] A significant barrier for applying the MC method to calculating image data is the high computational costs for sampling large numbers of photons in turbid media, which is needed to reduce the variance of the output distributed over, typically, 10^4 pixels or voxels. We have shown recently, however, that the computational time for tracking up to 10^8 photons for modeling reflectance images can be reduced to about 10 min or less with a computing cluster of sixteen 3.06 GHz CPUs using a optimized algorithm and the parallel coding technique.[11,14] Despite such progress, it is still extremely useful to have a closed-form solution for the reflectance imaging problem other than the MC method for rapid determination or estimation of parameters from the measured data. A rapid solution, even with errors within certain bounds, could serve two purposes: it may be used to reduce the cost-of-search in parameter space from the initial estimate made prior to accurate but expensive calculations such

as the MC simulations. It may also help resolve the inverse problems by producing additional constraints.[15]

The diffusion approximation of the RTE can yield a closed-form solution for the reflectance signals from a semi-infinite turbid media as a rapid modeling tool. Groenhuis *et al.* reported the first results with a P_1 diffusion approximation to invert spatially resolved light reflectance data for absorption and reduced scattering coefficients with validation against a MC method.[16] The P_1 solution was further improved by other workers with superior boundary conditions to calculate reflectance signals measured with single optical fibers with an underlying condition that the source-detector distance has to be sufficiently large to justify the diffusion approximation.[17–23] In this article, we extend from the previous results to obtain a closed-form solution of reflectance image from semi-infinite homogeneous turbid media with a full-field illumination beam of arbitrary profile. The validity of such a diffusion solution has been examined against the MC method on semi-infinite media and measured results on finite samples. Besides its utility for reflectance imaging, this solution also provides an opportunity to look into the interesting question of source-detector distance effect on the solution accuracy since these distances are effectively zero in our cases.

II. METHODS OF MODELING

II.A. The diffusion method

The boundary-value problems based on a diffusion equation of P_1 approximation have been thoroughly investigated and solved by other researchers.[17–20,22] Here we extend these results to obtain a closed-form solution for reflectance image from a homogeneous semi-infinite turbid phantom of volume $\Lambda \subset E^3$ $(z>0)$ and plane boundary $\partial\Lambda \subset E^2$ $(z=0)$, where E^d denotes a d-dimensional space. A collimated incident light beam propagating in the $x-z$ plane can be expressed in general by its radiance distribution in air as

$$L_0(\mathbf{r},\mathbf{s}) = I_0(\rho,\psi)\,\delta(\alpha)\,\delta(\cos\beta - \cos\theta_0), \tag{1}$$

where $\mathbf{s}=\cos\alpha\sin\beta\mathbf{x}+\sin\alpha\sin\beta\mathbf{y}+\cos\beta\mathbf{z}$ is a directional unit vector, $\mathbf{r}=x\mathbf{x}+y\mathbf{y}+z\mathbf{z}$, $I_0(\rho,\psi)$ is the irradiance profile in the cross-sectional plane of the incident beam with ρ, ψ as the polar coordinates, δ is the Dirac delta function, and θ_0 is the incident angle, as shown in Fig. 1.

Within a source-free turbid medium, the light distribution is described by a radiance $L(\mathbf{r};\mathbf{s})$ satisfying a steady-state RT equation[24]

$$\mathbf{s}\cdot\nabla L(\mathbf{r},\mathbf{s}) = -(\mu_a+\mu_s)L(\mathbf{r},\mathbf{s}) + \mu_s\int_{4\pi} p(\mathbf{s},\mathbf{s}')L(\mathbf{r},\mathbf{s}')d\Omega' \;\forall\,\mathbf{r}\in\Lambda, \tag{2}$$

where μ_a and μ_s is the absorption and scattering coefficients, respectively, and $p(\mathbf{s},\mathbf{s}')$ is the scattering phase function related to the probability for a photon to be scattered from $\mathbf{s}'$ to $\mathbf{s}$. For axial symmetric scattering, an anisotropy factor g can be defined as the first moment of the phase function, $g=\int_{4\pi}p(\cos\Theta)\cos\Theta d\Omega$, to characterize the deviation of the scattering events from an isotropic distribution with $\cos\Theta=\mathbf{s}\cdot\mathbf{s}'$. By dividing the radiance $L(\mathbf{r};\mathbf{s})$ into a primary component L_p and a scattered component L_s, the RT equation can be separated into two equations with one for each component.[24] The primary component can be solved as

$$L_p(\mathbf{r},\mathbf{s}) = L_{pu}(\mathbf{r},\mathbf{s})\exp\left(-\int_0^d \mu_t ds\right) = L_{pu}(\mathbf{r},\mathbf{s})\exp(-\mu_t z/\cos\theta), \tag{3}$$

for homogeneous turbid medium with θ as the refraction angle determined from $\sin\theta_0=n\sin\theta$ and $d=z/\cos\theta$ as the pathlength of refracted light in the medium from the boundary $\partial\Lambda$ to $\mathbf{r}$ along $\mathbf{s}$ (see Fig. 1). By considering the energy balance at $\partial\Lambda$, we find the unattenuated portion of the primary component in Λ to be

$$L_{pu}(\mathbf{r},\mathbf{s}) = I_{\max}p(x-z\tan\theta,y)[1-R_{\text{Fresnel}}(\theta_0)] \times\delta(\alpha)\,\delta(\cos\beta-\cos\theta)\frac{\cos\theta_0}{\cos\theta}, \tag{4}$$

where $I_{\max}$ is the maximum value of $I_0(\rho,\psi)$, $p(x,y)$ is the normalized profile of the incident beam projected and stretched along the x axis by a factor of $1/\cos\theta_0$ at $\partial\Lambda$, and R_{Fresnel} is the unpolarized Fresnel reflection coefficient given by

$$R_{\text{Fresnel}}(\theta_0) = \frac{1}{2}\left(\frac{\cos\theta - n\cos\theta_0}{\cos\theta + n\cos\theta_0}\right)^2 + \frac{1}{2}\left(\frac{\cos\theta_0 - n\cos\theta}{\cos\theta_0 + n\cos\theta}\right)^2. \tag{5}$$

Compared to the projected irradiance profile of $I_{\max}(\cos\theta_0)p(x,y)(1-R_{\text{Fresnel}})$ at $z=0$, the beam profile of the primary component inside Λ along the θ direction, or the refracted beam, is translated by $z(\tan\theta)$ as the refracted beam propagates.

The equation for $L_s(\mathbf{r},\mathbf{s})$ is difficult to solve and often a P_1 approximation is employed to obtain a diffusion equation by keeping only the first two terms ($l=0$ and 1) in the spherical harmonic expansion of $L_s(\mathbf{r},\mathbf{s})$,[24,25]

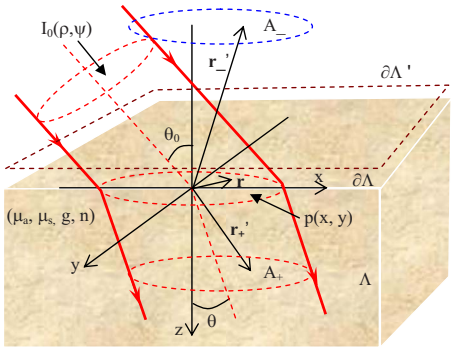

FIG. 1. The schematic of the tissue phantom configuration with the incident beam. The dash lines represent the profiles of the incident beam in the air (I_0) and its projection at the phantom surface ($z=0$), the source disk in the phantom due to the primary component (A_+) and the image source disk (A_-). All other parameters are defined in the text.

$$L_s(\mathbf{r},\mathbf{s}) \approx \frac{1}{4\pi}\{\Phi(\mathbf{r}) + 3\mathbf{F}(\mathbf{r})\cdot\mathbf{s}\}, \tag{6}$$

where $\Phi(\mathbf{r})=\int_{4\pi}L_s(\mathbf{r},\mathbf{s})d\Omega$ and $\mathbf{F}(\mathbf{r})=\int_{4\pi}L_s(\mathbf{r},\mathbf{s})\mathbf{s}d\Omega$. Substitution of $L_s(\mathbf{r},\mathbf{s})$ by the fluence rate $\Phi(\mathbf{r})$ and net flux vector $\mathbf{F}(\mathbf{r})$ into the RT Eq. (2), with rearrangement and simplification, eventually leading to a second-order differential equation of diffusion type on $\Phi(\mathbf{r})$,[24]

$$\nabla\cdot\{D\,\nabla\,\Phi(\mathbf{r})\} - \mu_a\Phi(\mathbf{r}) = -S_p(\mathbf{r}), \tag{7}$$

where

$$S_p(\mathbf{r}) = \mu_s\Phi_p(\mathbf{r}) + 3\,\nabla\,\cdot D\mu_s\int_{4\pi}\int_{4\pi}\mathbf{s}p(\mathbf{s},\mathbf{s}')L_p(\mathbf{r},\mathbf{s}')d\Omega' d\Omega \tag{8}$$

acts as a source term due to scattering of the primary component, $D=1/3[\mu_a+(1-g)\mu_s]$, which is the diffusion coefficient and $\Phi_p(\mathbf{r})=\int_{4\pi}L_p(\mathbf{r},\mathbf{s})d\Omega$, which is the fluence rate of the primary component.

A partial-current boundary condition at $\partial\Lambda$ (Ref. 20) can be used with Eq. (7) to define a boundary-value problem for solving $\Phi(\mathbf{r})$ within the phantom volume Λ, as shown in the Appendix. This allows the calculation of the reflectance image $R_D(x,y)$ at the boundary $\partial\Lambda$ as a ratio of reflected irradiance $I_R(x,y)$ to that of the incident beam at $\partial\Lambda$, i.e.,

$$R_D(x,y) = \frac{I_R(x,y)}{I_{\max}\cos\,\theta_0}. \tag{9}$$

Again, using the diffusion approximation of Eq. (6) and the Fick's law, we find

$$I_R(x,y) = \int_{\mathbf{s}\cdot\mathbf{z}<0}[1-R_{\text{Fresnel}}(\mathbf{s})]L_s(\mathbf{r},\mathbf{s})(-\mathbf{s}\cdot\mathbf{z})|_{z=0}d\Omega,$$

$$= \frac{1}{2}\int_0^{\theta_c}\{1-R_{\text{Fresnel}}(\theta_i)\} \times\left\{\Phi(\mathbf{r}) + 3D\frac{\partial\Phi(\mathbf{r})}{\partial z}\cos\,\theta_i\right\}\Big|_{z=0}\cos\,\theta_i\sin\,\theta_i d\theta_i, \tag{10}$$

where θ_c is the critical angle determined by $\sin\,\theta_c=1/n$. From the fluence rate $\Phi(\mathbf{r})$ given in Eq. (A6), the normal derivative can be found as

$$\frac{\partial\Phi(\mathbf{r})}{\partial z}\Big|_{z=0} = \frac{\mu_s'}{\mu_t'}\frac{[1-R_{\text{Fresnel}}(\theta_0)]I_0\cos\,\theta_0}{4\pi D} \times\{\mu_{\text{eff}}A_2(x,y;z_c,z_b) + A_3(x,y;z_c,z_b)\}, \tag{11}$$

with

$$A_i(x,y;z_c,z_b) = \int_A\left\{\frac{z_c\exp[-\mu_{\text{eff}}\sqrt{(x-x')^2+(y-y')^2+z_c^2}]}{[\sqrt{(x-x')^2+(y-y')^2+z_c^2}]^i} + \frac{(z_c+2z_b)\exp[-\mu_{\text{eff}}\sqrt{(x-x')^2+(y-y')^2+(z_c+2z_b)^2}]}{[\sqrt{(x-x')^2+(y-y')^2+(z_c+2z_b)^2}]^i}\right\}pda', \tag{12}$$

for $i=2,3$. Substitution of Eqs. (A6) and (11) into Eq. (9) produces the reflectance image

$$R_D(x,y) = \frac{\mu_s'[1-R_{\text{Fresnel}}(\theta_0)]}{\mu_t' 4\pi D}\{c_1A_1 + 3c_2D[\mu_{\text{eff}}A_2 + A_3]\}, \tag{13}$$

where

$$A_1 = \int_A\left\{\frac{\exp[-\mu_{\text{eff}}\sqrt{(x-x')^2+(y-y')^2+z_c^2}]}{\sqrt{(x-x')^2+(y-y')^2+z_c^2}} - \frac{\exp[-\mu_{\text{eff}}\sqrt{(x-x')^2+(y-y')^2+(z_c+2z_b)^2}]}{\sqrt{(x-x')^2+(y-y')^2+(z_c+2z_b)^2}}\right\}pda', \tag{14}$$

and

$$c_j = \frac{1}{2}\int_{\cos\,\theta_c}^1[1-R_{\text{Fresnel}}(\theta_i)]\cos^j\,\theta_i d\cos\,\theta_i, \tag{15}$$

with $j=1,2$.

To increase the accuracy of R_D based on Eq. (13) for modeling of reflectance image data, the normalized incident beam profile $p(x,y)$ over the field-of-view (FOV) at $\partial\Lambda$ can be imported from a reflectance image measured with a diffuse reflectance standard. The FOV at $\partial\Lambda$ and the two source disks of A_+ and A_- are typically divided with the same grid of N_g cells, so the computational cost of an R_D image over the FOV is $O(N_g^2)$.

II.B. The MC method

A MC method has been developed and validated extensively to calculate the light distribution in terms of a photon density function within the framework of RTE and Fresnel's equations with details published elsewhere.[11,12,26] A one-parameter Henyey–Greenstein function, $p_{\text{HG}}(\cos\,\Theta)$, is used as the phase function in all MC simulations. An incident beam of N_0 photons is distributed at the plane surface of $\partial\Lambda$ according to the projected beam profile $p(x,y)$. Photons entered into a turbid medium are tracked individually along their trajectory in the MC code.[7,9] A fast MC algorithm has

been developed[11] in which a life pathlength L_a and free pathlength L_s of the tracked photon in the turbid medium is first determined by random numbers of exponential distributions with mean values, among all tracked photons, given by $\langle L_a \rangle = 1/\mu_a$ and $\langle L_s \rangle = 1/\mu_s$, respectively, before tracking starts. For heterogeneous media, the residue pathlengths are rescaled as the tracked photon enters a region of different μ_a and μ_s to handle heterogeneity.[10,14] Other parts of the algorithm are similar to those described in Ref. 9. If a tracked photon is incident on an interface between two regions of different refractive indices, the Fresnel reflectivity R_{Fresnel} given in Eq. (5) is calculated and used to determine if the photon reflects from, or transmits through, the interface by comparing it to a random number.[12]

After all incident photons of $N_0[1-R_{\text{Fresnel}}(\theta_0)]$ are tracked, we obtain from the MC output the surface density distributions or the number of remitted photons per grid cell at the air side of surface $\partial\Lambda$, $\rho_R(x,y)$, over the FOV. The reflectance image $R_{\text{MC}}(x,y)$ is then calculated from the following:

$$R_{\text{MC}}(x,y) = \frac{\rho_R(x,y)}{\rho_{\max} \cos\theta_0}, \tag{16}$$

where $\rho_{\max}$ is the maximum photon surface density of the incident beam. To study the dependence of the reflected light signals on the number of scattering events, multiple outputs are obtained from each MC simulation according to the number of scattering events m experienced by the remitted photons registered for a reflectance image. For example,

$$R_{\text{MCm}}(x,y) = \frac{\rho_{Rm}(x,y)}{\rho_{\max} \cos\theta_0}, \tag{17}$$

is defined as the reflectance contributed by those photons scattered m or more times. The MC simulation time scales linearly with N_0 due to the requirement of fluctuation in $\rho_R(x,y)$ being kept at 2% or less.[10,14] Therefore, the computational cost of an R_{MC} image over the FOV is $O(N_g)$.

III. EXPERIMENTAL METHODS

A light beam from a noncoherent light source (DC950, Dolan-Jenner) was used to project a pattern structure onto the surface of a homogeneous turbid sample after an interference filter of 10 nm bandwidth with wavelength λ selectable from 500 to 1000 nm. The center axis of the incident beam intersects with sample surface at an incident angle θ_0 with a small diverging angle of 1.9°. Homogeneous turbid samples have been made as tissue phantoms with TiO_2 powders (213581000, Across Organics) and different concentrations of brown pigment powders (Pbr7, Kama Pigments) suspended in silicone polymer (RTV615A, MG Chemicals). The suspensions were stirred for 5 days to ensure suspension homogeneity during the sample preparation process through solidification with hardener. Each type of samples consists of one large disk of 40 mm in diameter and 10 mm in thickness for reflectance imaging and multiple thin disks of 18 mm in diameter and 0.1–1 mm in thickness for determination of optical parameters with an integrating sphere based method.[26] Care was taken to make the same type samples out of the same suspension with uniform thickness.

We employed a thermoelectrically cooled 16-bit charge coupled device (CCD) camera (ST-7, SBIG), oriented along the normal direction of the sample surface, to measure images $I_{mr0}(x,y)$ of reflected light at λ with a camera lens of 25 mm focal length. The imaging system was aligned so that CCD sensor plane is conjugate to the sample surface. Another image $I_{ms0}(x,y;\lambda)$ was acquired from a diffuse reflectance standard of calibrated reflectance R_s (Labsphere, Inc.) in the place of sample to determine the normalized incident beam profile $p(x,y)$ projected on the reflected surface. All images were cropped and pixel binned to produce a FOV of 25.7×19.5 mm^2 with a 67×51 pixel grid for rapid generation of calculated images. Separate background images of $I_{mrb}(x,y)$ and $I_{msb}(x,y)$ from the sample and reflectance standard, respectively, were obtained with the incident beam blocked to subtract the read-out and dark current noises from all acquired images. The background-free images, $I_i(x,y) = I_{i0}(x,y) - I_{ib}(x,y)$, with $i=mr$ or ms, were used to construct a measured reflectance image of $R_m(x,y) = I_{mr}(x,y)R_s/I_{\max,s}$ and a normalized profile image of $p(x,y) = I_s(x,y)/I_{\max,s}$ for the incident beam, where $I_{\max,s}$ is the maximum pixel value of the image $I_{ms}(x,y)$.

IV. RESULTS

We first compared the calculated reflectance images obtained according to Eqs. (13) and (16) for an incident beam at varying θ_0. The beam profile $I_0(\rho,\psi)$ was first assumed to be circular with a top-hat profile of radius $w=12.5$ mm, i.e., $I_0(\rho,\psi) = I_{\max}$ for $\rho \leq w$ and 0 otherwise. For this case we employed a FOV of 60×60 mm^2 divided by a 101×101 grid. For MC results, reflectance images R_{MC} or $R_{\text{MC}m}$ were averaged over five rows centered on the x axis to reduce output variance in the presented results of $R(x,0)$. The MC simulations were performed on a computing cluster of eight nodes of dual Intel xeon CPU of 3.06 GHz using a parallel code.[14] The incident photon number was fixed at $N_0 = 1.2 \times 10^9$ photons for all MC simulations with wall-clock time varying from about 3 min in the cases of small albedo $a = \mu_s/\mu_t$ ($\mu_a = 0.75$ mm^{-1}, $\mu_s = 3.00$ mm^{-1}) to about 67 min in the cases of large a ($\mu_a = 0.01$ mm^{-1}, $\mu_s = 5.00$ mm^{-1}). In comparison, each calculation of the reflectance image with the diffusion solution, based on Eq. (13), took about 1 min on 1 CPU of the same computing cluster for the above grid.

The reflectance image results for a turbid medium of small anisotropy factor g with $\mu_a = 0.01$ mm^{-1}, $\mu_s = 5.00$ mm^{-1}, $g=0.20$, and $n=1.40$ are presented in Fig. 2(a) for $\theta_0 = 0$. A relative error δ is defined to represent the difference in reflectance images between either the diffusion solution or MC method $m>1$, and the MC method with $m=1$, i.e.,

$$\delta(x,0) = \frac{R(x,0) - R_{\text{MC}}(x,0)}{R_{\text{MC}}(x,0)}, \tag{18}$$

where $R(x,0)$ is either $R_D(x,0)$, $R_{\text{MC3}}(x,0)$, or $R_{\text{MC5}}(x,0)$. The relative errors from the calculated reflectance image pro-

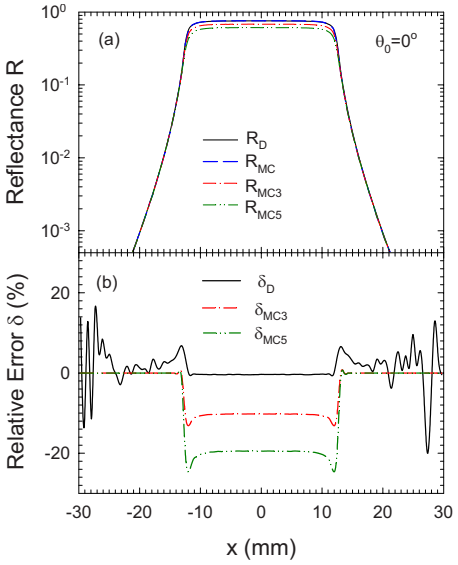

FIG. 2. Reflectance images calculated with an incident beam of top-hat profile: (a) $R(x,0)$ calculated by the diffusion and MC methods with different registration of scattered photons: all internally scattered photons ($m=1$), only those scattered three times or more than ($m=3$) and only those scattered five times or more ($m=5$); (b) the relative reflectance error δ of diffusion solution in comparison to the MC calculated R with $m=1$. The optical parameters of the phantom are $\mu_a=0.01$ mm^{-1}, $\mu_s=5.00$ mm^{-1}, $g=0.20$, and $n=1.40$ at $\theta_0=0°$.

files shown in Fig. 2(a) are plotted in Fig. 2(b). The relative errors with incident beam at oblique incidence angles of $\theta_0=30°$ and 60° and the same turbid medium are presented in Fig. 3. Large fluctuations in relative error δ at the edges of the illumination zone are due to the large variance in R_{MC} where the numbers of remitted photons per grid cell become less than 10.

It can be seen from the above results that the diffusion solution derived in this article can produce quite accurate

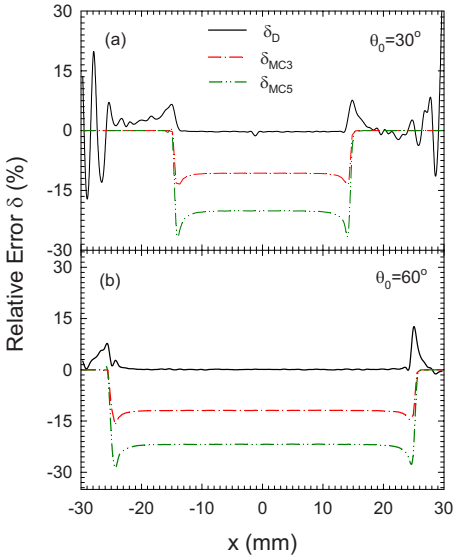

FIG. 3. The relative error of reflectance δ in comparison to the MC calculated results with $m=1$ with same optical parameters in Fig. 2 for a top-hat incident beam at $\theta_0=30°$ and 60°.

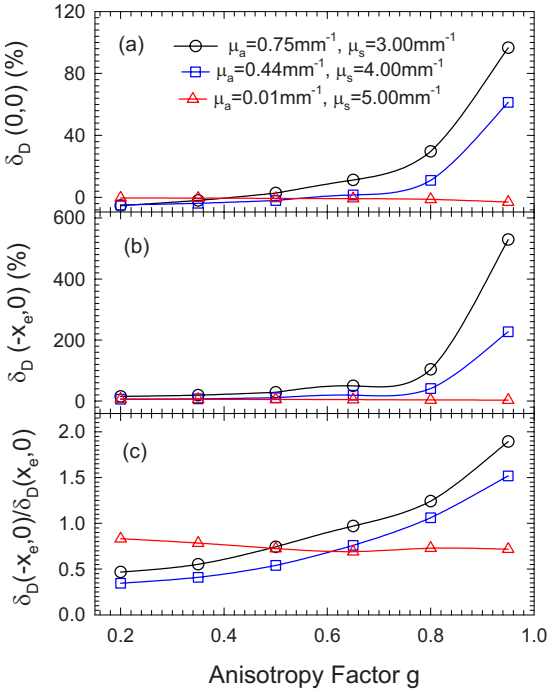

FIG. 4. The relative error of reflectance δ_D at the center ($x=0$), negative ($x=-x_e$) and positive ($x=-x_e$) edges with $x_e=14.9$ mm vs the anisotropy factor of the tissue phantom at different values of albedo $a=99.8\%$, 90.1%, and 80.0%, $n=1.40$ using a top-hat incident beam at $\theta_0=30°$. The solid lines are for visual guide.

reflectance images within the illumination zone for a top-hat beam profile in comparison to the MC method for phantoms with a small anisotropy factor g. The relative error δ_D between the two methods increases at the edges of the illumination zone $x=\pm x_e$. Therefore, the profile difference between the two methods of modeling for reflectance images can be well represented by the value of δ_D at the center ($x=0$), averaged between $x=-5$ and 5 mm, and its peak values at $\pm x_e$. Figure 4 shows the relative error δ_D at these three locations versus the anisotropy factor g for phantoms of different albedo a.

We examined the validity of the diffusion method for modeling reflectance images against the MC method with measured beam profiles and images from turbid samples. Since an incident beam with a profile close to "top-hat" would require homogenizing the beam with several sanded glass diffusers, we chose to employ two profiles of "Gaussian-like" of single-peak and grating, as shown in Fig. 5 with a diffuse reflectance standard of $R_s=20\%$. Each of the measured beam profiles was normalized and imported into the numerical codes as $p(x,y)$ to improve modeling accuracy of reflectance images. For the single-peak profile, the differences in the reflectance images from a semi-infinite medium between the diffusion and MC methods are similar to those calculated with the ideal top-hat profile, as presented in Fig. 6. In Fig. 7 we plotted the reflectance image profile calculated by the diffusion solution for semi-infinite medium and the MC method for both semi-infinite and finite sized phantoms with a grating beam profile in two cases of g values to

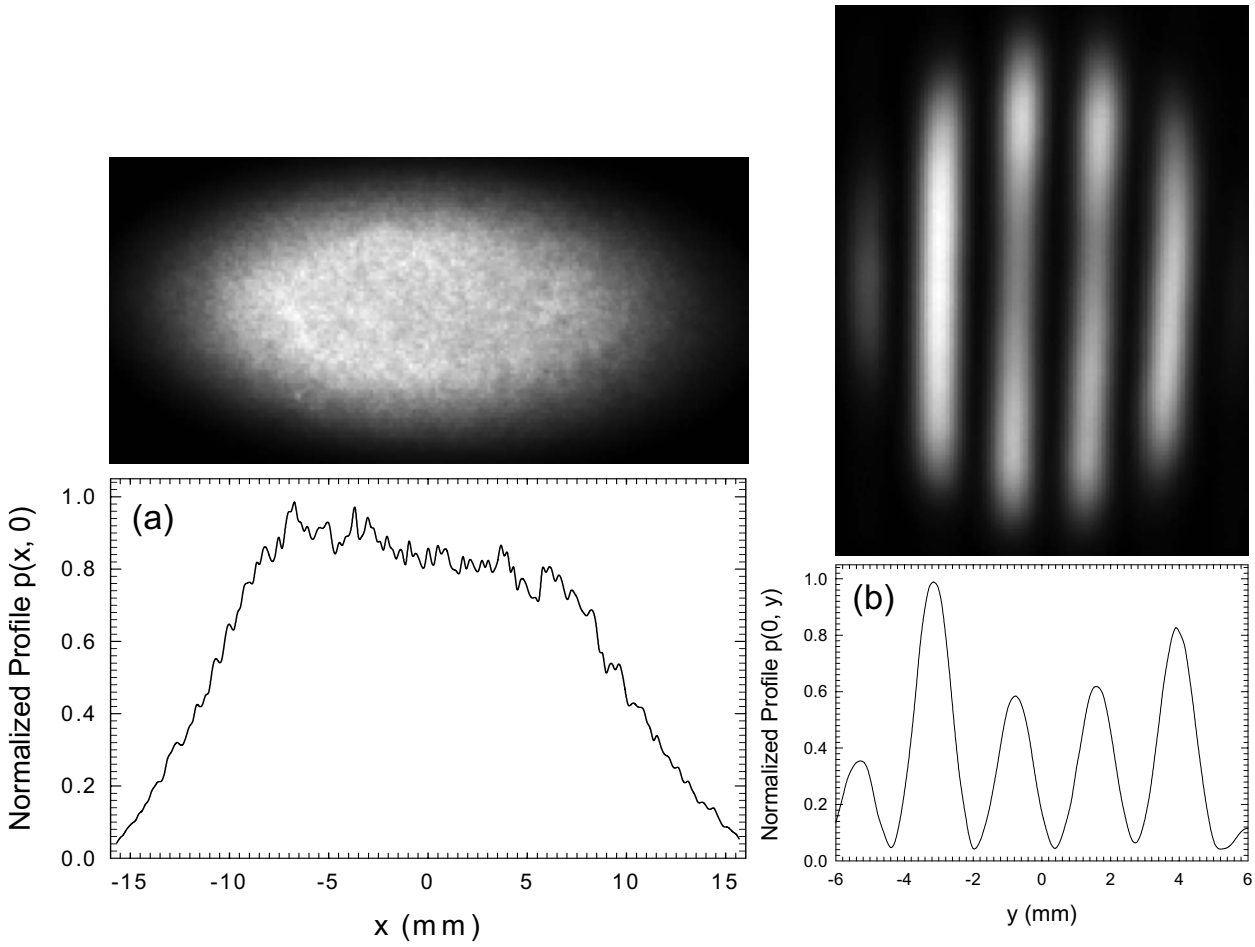

FIG. 5. Two incident beam profiles measured with a 20% diffuse reflectance standard and normalized beam profile $p(x,0)$ or $p(0,y)$: (a) a single-peak beam at $\theta_0=60°$ and (b) a grating beam at $\theta_0=45°$.

illustrate the effect of side boundary in a finite sized phantom. Finally, the reflectance images calculated with the two methods and measured from one homogeneous turbid sample are shown in Fig. 8 using the optical parameters determined from its thin disk copies by an integrating sphere based method at $\lambda=560$ nm. The largest relative errors of modeling, for either diffusion or MC method in comparison with the measured data, occur at the minimum of reflectance at about 35%.

V. DISCUSSION

Reflectance imaging of turbid media with a full-field illumination provides a simple method to characterize turbid media without contact and thus has significant potentials for various applications, especially as a tool for noninvasive diagnosis in medicine. With an accurate model of tissue optics, the reflectance image data can be used to determine the optical parameters of the imaged medium.[15,26] For media with complex heterogeneity and/or irregularly shaped boundary, the MC simulation is often a method of choice for its accuracy within the radiative transfer theory and algorithmic simplicity, but computational cost remains a barrier.[12,14] Despite its limitation to solve problems of heterogeneous turbid media, diffusion approximations of the RT equation can yield closed-form solutions for the cases of homogeneous turbid media and thus is very useful in generating partial and/or initial estimates of parameters as a part of the modeling toolbox. In this article we derived a diffusion solution in P_1 approximation for modeling of reflectance images from homogeneous semi-infinite media illuminated by an incident beam of arbitrary profile at oblique angles.

The results presented in Fig. 4, for an ideal top-hat incident beam, demonstrate that even for g values as large as 0.7 the diffusion solution produces accurate reflectance image data for highly turbid phantoms with albedo $a>0.90$ using the isotropic disk source terms [see Eq. (A5)] for the fluence rate Φ. But for media of modest a, 80% or less, the difference between diffusion and MC results increases steeply with g, especially at the edges of the illuminated zone, as shown in Figs. 4(a) and 4(b). These large errors at the edges can be attributed to the adoption of the similarity principle based on a P_1 diffusion approximation given by Eq. (6), which neglects the anisotropic portion of the source term. This is corroborated by the results presented in Fig. 4(c) in which the overestimated reflectance by the diffusion solution at $-x_e$ overtakes that at x_e as g increases toward 1, since the former corresponds to the backward scattering directions while the latter to the forward directions. Comparison of the

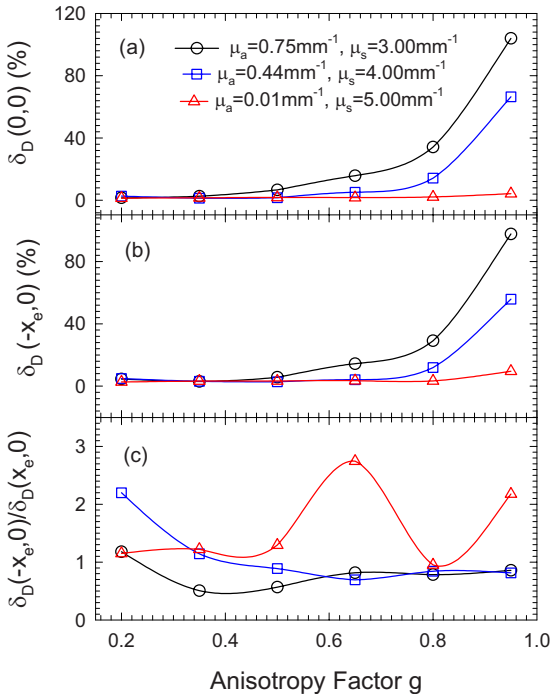

FIG. 6. The relative error of reflectance δ_D at the center (x=0), negative (x=$-x_e$) and positive (x=$-x_e$) edges with x_e=12.8 mm vs the anisotropy factor of the tissue phantom at different values of albedo a=99.8%, 90.1%, and 80.0%, n=1.40 using the measured profile of incident beam shown in Fig. 5(a) at θ_0=60°. The solid lines are for visual guide.

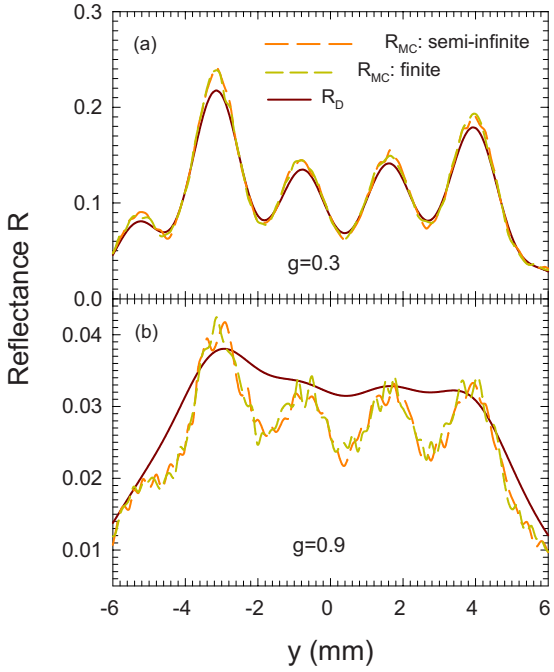

FIG. 7. Reflectance images R calculated by the diffusion and MC methods with the measured profile of incident beam shown in Fig. 5(b): (a) g=0.30; (b) g=0.90. The diffusion and MC results were obtained for semi-infinite and finite phantoms with optical parameters using μ_a=0.18 mm^{-1}, μ_s=3.95 mm^{-1}, and n=1.41 as determined by an integrating sphere based method at λ=56 nm (Ref. 26). The finite phantom is of cylinder shape with 40 mm diameter and 10 mm thickness.

results plotted in Figs. 4 and 6 reveals that the beam profile itself has little effect on the accuracy of our diffusion solution. In fact, the gradual change in the profile of the single-peak beam leads to a smaller error in the diffusion solution than in the case of top-hat profile. Obviously, use of a measured profile instead of an artificial top-hat or Gaussian profile for the incident beam can significantly improve the accuracy of the calculated reflectance images for both diffusion and MC methods. We also note from our MC results (with only two cases presented in Fig. 7) that the boundary of a finite sized sample does not affect the modeling accuracy as long as the boundary is several mean transportation free length L_{tr} away from the FOV. This suggests that in these cases the diffusion solution derived here for a semi-infinite turbid medium is sufficiently accurate for rapid modeling of image data from finite sized samples of appropriate values of a and g if the sample size is large. Finally, the results shown in Figs. 7 and 8 demonstrate that even for an incident beam with a structured profile, the diffusion solution can provide reasonably accurate modeling of the measured reflectance images for g=0.30 or 0.56. In comparison, for cases of large g values as shown in Fig. 7(b), the diffusion solution ceases to be a valid model. It becomes clear from these results that the diffuse solution presented in this report can be used as a reasonably accurate tool for the modeling of reflectance images with full-field illumination for homogeneous turbid media of g<0.7 and a>0.8, with an increasing accuracy for large a.

Unlike the fiber based methods, a reflectance image consists of reflected light signals or photons from the same illumination zone and thus has an effectively zero source-detector distance. In this situation one would expect a poor performance of diffusion model since the detected photons may not have chances to become sufficient diffused through multiple scattering, contrary to what we shown here. As shown in Figs. 2(b) and 3, a small but not insignificant percentage, 10%–15%, of reflectance image signals is due to those photons being scattered only once or twice. This percentage can increase quite rapidly if the scattering albedo a

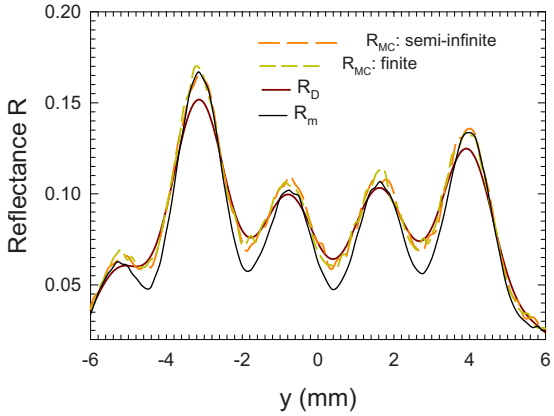

FIG. 8. Reflectance images R same as Fig. 7 except using g=0.56 as determined by an integrating sphere based method (Ref. 26) and addition of the measured data.

decreases from the high value of 99.8% in the above case. Therefore, the value of g has to be small enough to ensure that the detected photons distribute isotropically after two or more scatterings. The requirement of $g<0.7$ for the diffusion solution to be valid, demonstrated by our results, yields an averaged scattering angle of 45° or larger and thus agrees with the above considerations. We should note here that none of the calculated images in Fig. 8 agrees very well with the measured image since they were obtained using the optical parameters determined from thin copies of the sample material with an integrating sphere based method,[26] indicating that the optical parameters determined by these two methods can deviate slightly. A systematic study is currently underway to develop a reflectance image based inverse method for determination of optical parameters and validate against the established integrating sphere based method, which requires both reflectance and transmittance data. Results will be published soon.

We also analyzed the contribution to the diffusely reflected light by photons undergoing different numbers of scattering events to investigate the possibility of a hybrid modeling scheme that has been proposed by different researchers for reducing the MC simulation time.[27–29] With our choice of the light source term in the diffusion equation, however, the diffusion solution produced overestimated reflectance in comparison to the MC results in most of the considered cases, as shown in Figs. 2 and 3. Therefore, a hybrid model, using the diffusion modeling technique, would not work properly here as proposed in[27,28] to eliminate tracking of photons undergoing large number of scattering events in the MC method. The difference between our and previous results is due to the choice of source term in the diffusion equation [see Eqs. (7) and (8)]. This fact underscores the large degree of arbitrariness in developing a diffusion solution in addition to the requirements of large albedo and small anisotropy factor. Therefore, the usefulness of a hybrid models is quite limited, if ever useful.

ACKNOWLEDGMENT

The authors thank Kenneth M. Jacobs for help on construction of turbid samples and the reflectance imaging system.

APPENDIX: SOLUTION OF THE BOUNDARY-VALUE PROBLEM WITH A FULL-FIELD ILLUMINATION

Several boundary conditions have been proposed and studied for diffusion approximation. Among these, an extrapolated boundary condition based on a partial-current concept has been shown capable of yielding a closed-form solution of reasonable accuracy.[17,18,20,22] The partial-current concept equates the light irradiance at the boundary plane $\partial\Lambda$, propagating toward the inside of the phantom, to the reflected portion of the scattered radiance propagating toward the boundary. Adopting the symbols used in Ref. 20, this can be expressed as

$$\int_{\mathbf{s}\cdot\mathbf{z}>0} L_s(\mathbf{r},\mathbf{s})(\mathbf{s}\cdot\mathbf{z})d\Omega = \int_{\mathbf{s}\cdot\mathbf{z}<0} R_{\text{Fresnel}}(\mathbf{s})L_s(\mathbf{r},\mathbf{s}) \times(-\mathbf{s}\cdot\mathbf{z})d\Omega. \tag{A1}$$

Using Eq. (6) and the Fick's law of $\mathbf{F}(\mathbf{r})=-D\nabla\Phi(\mathbf{r})$ for the scattered component, it has been shown that Eq. (A1) yields a mixed, or type III, boundary condition[20]

$$\Phi(\mathbf{r}) = z_b\frac{\partial\Phi(\mathbf{r})}{\partial z} \quad \forall\,\mathbf{r}\in\partial\Lambda, \tag{A2}$$

where $z_b=2D[(1+R_{\text{eff}})/(1-R_{\text{eff}})]$, $R_{\text{eff}}=[(R_F+R_\Phi)/(2+R_F-R_\Phi)]$, $R_\Phi=\int_0^{\pi/2}2R_{\text{Fresnel}}(\theta_i)\sin\theta_i\cos\theta_i d\theta_i$ and $R_F=\int_0^{\pi/2}3R_{\text{Fresnel}}(\theta_i)\cos^2\theta_i\sin\theta_i d\theta_i$ with θ_i referring to the incident angle of $L_s(\mathbf{r},\mathbf{s})$ propagating toward $\partial\Lambda$. For the parameter ranges relevant to human tissue, z_b is typically between 0.1 and 1 mm, a distance much smaller than the phantom sizes considered here. Therefore, the boundary condition can be further approximated as a type I or Dirichlet condition of $\Phi(\mathbf{r})=0$ at an "extrapolated boundary" of $\partial\Lambda'$ at $z=-z_b$. So the boundary-value problem for the homogeneous medium depicted in Fig. 1 under the diffusion approximation can be written as

$$\begin{cases}\nabla^2\Phi(\mathbf{r})-\mu_{\text{eff}}^2\Phi(\mathbf{r})=-\dfrac{S_p(\mathbf{r})}{D} & \forall\,\mathbf{r}\in\Lambda,\\ \Phi(\mathbf{r})=0 & \forall\,\mathbf{r}\in\partial\Lambda',\end{cases} \tag{A3}$$

where $\mu_{\text{eff}}=(\mu_a/D)^{1/2}$.

Equation (A3) can be solved with a method of images in which the effect of the boundary condition on $\Phi(\mathbf{r})$ can be represented by an image, at $\mathbf{r}_-=\mathbf{r}_+-(2z_+-2z_b)\mathbf{z}$, of the source S_p at $\mathbf{r}_+=x_+\mathbf{x}+y_+\mathbf{y}+z_+\mathbf{z}$. The solution is then given by that of the same diffusion equation in all space in the form of a Green function $G(\mathbf{r};\mathbf{r}'_+,\mathbf{r}'_-)$,

$$\begin{aligned}\Phi(\mathbf{r}) &= \int_{\text{all space}} G(\mathbf{r};\mathbf{r}'_+,\mathbf{r}'_-)S_p(\mathbf{r}')d^3r'\\ &= \frac{1}{4\pi D}\left\{\int_{z'>0}\frac{S_p(\mathbf{r}'_+)e^{-\mu_{\text{eff}}|\mathbf{r}-\mathbf{r}'_+|}}{|\mathbf{r}-\mathbf{r}'_+|}d^3r'_+ - \int_{z'<0}\frac{S_p(\mathbf{r}'_-)e^{-\mu_{\text{eff}}|\mathbf{r}-\mathbf{r}'_-|}}{|\mathbf{r}-\mathbf{r}'_-|}d^3r'_-\right\}.\end{aligned} \tag{A4}$$

The source term S_p defined in Eq. (8) can be simplified with two techniques. Under the P_1 approximation, light distribution in a turbid medium depends only on μ_a and $\mu'_s=\mu_s(1-g)$ and therefore any anisotropic medium with (μ_a,μ_s,g) can be treated equivalently as an isotropic one with $(\mu_a,\mu'_s,0)$.[30] This eliminates the second term in Eq. (8). In addition, S_p is due to the first scattering of the primary component $L_p(\mathbf{r}'_+)$ which exists as an oblique "pipe" inside the turbid medium, as shown in Fig. 1. It has been previously proposed that the source term associated with the primary component of a "pencil" beam can be replaced by a point source, located at one mean transportation free length $L_{\text{tr}}(=3D)$ from the boundary, on the straight line trajectory of the primary photons.[19,22] Following this strategy, we replace

the pipe associated with S_p by a disk A_+ of same refracted beam profile which is stretched along the x axis relative to the incident beam profile and centered at $(x_c,0,z_c)$, where $z_c=\cos\theta/\mu_t'$, $x_c=z_c\tan\theta=\sin\theta/n\mu_t'$ and $\mu_t'=\mu_a+\mu_s'$. With these considerations, we finally obtain a simplified form of the source term defined in Eq. (8) as a "single disk"

$$S_{pd}(\mathbf{r}_+')=\mu_s'\int_{4\pi}L_p(\mathbf{r},\mathbf{s})d\Omega=\frac{\mu_s'}{\mu_t'}I_{\max}p(x_+'-z_c\tan\theta,y_+')\times[1-R_{\text{Fresnel}}(\theta_0)]\cos\theta_0\delta(z_+'-z_c),\tag{A5}$$

where a factor of $1/\mu_t'$ was used to ensure that $\int_0^\infty S_p(\mathbf{r})dz=\int_0^\infty S_{pd}(\mathbf{r})dz$. With the simplified source S_{pd} replacing S_p, the solution of the boundary-value problem given in Eq. (A3) then becomes

$$\Phi(r)=\frac{\mu_s'}{\mu_t'}\frac{[1-R_{\text{Fresnel}}(\theta_0)]I_{\max}\cos\theta_0}{4\pi D}\times\int_A\left\{\frac{\exp[-\mu_{\text{eff}}|\mathbf{r}-\mathbf{r}_+'|]}{|\mathbf{r}-\mathbf{r}_+'|}-\frac{\exp[-\mu_{\text{eff}}|\mathbf{r}-\mathbf{r}_-'|]}{|\mathbf{r}-\mathbf{r}_-'|}\right\}pda',\tag{A6}$$

where the area integrals in A are to be carried out on the source disk A_+ and its image A_-. The source disks are sketched in Fig. 1 by the red dashed lines in Λ for A_+ and blue dashed lines in air for A_- outside of Λ relative to the extrapolated boundary $\partial\Lambda'$. Both area integrals are convolved with the stretched and translated beam profile $p(x_\pm'-z_c\tan\theta,y_\pm')$.

[a]Author to whom correspondence should be addressed. Electronic mail: hux@ecu.edu

[1]S. L. Jacques, J. C. Ramella-Roman, and K. Lee, "Imaging skin pathology with polarized light," J. Biomed. Opt. **7**, 329–340 (2002).
[2]A. N. Yaroslavsky, V. Neel, and R. R. Anderson, "Fluorescence polarization imaging for delineating nonmelanoma skin cancers," Opt. Lett. **29**, 2010–2012 (2004).
[3]I. Nishidate, Y. Aizu, and H. Mishina, "Depth visualization of a local blood region in skin tissue by use of diffuse reflectance images," Opt. Lett. **30**, 2128–2130 (2005).
[4]J. T. Bruulsema, J. E. Hayward, T. J. Farrell, M. S. Patterson, L. Heinemann, M. Berger, T. Koschinsky, J. Sandahl-Christiansen, H. Orskov, M. Essenpreis, G. Schmelzeisen-Redeker, and D. Ba Cker, "Correlation between blood glucose concentration in diabetics and noninvasively measured tissue optical scattering coefficient," Opt. Lett. **22**, 190–192 (1997).
[5]G. Zonios, J. Bykowski, and N. Kollias, "Skin melanin, hemoglobin, and light scattering properties can be quantitatively assessed in vivo using diffuse reflectance spectroscopy," J. Invest. Dermatol. **117**, 1452–1457 (2001).
[6]J. Lenoble, *Radiative Transfer in Scattering and Absorbing Atmospheres: Standard Computational Procedures* (A. Deepak, Hampton, VA, 1985).
[7]G. I. Marchuk, *The Monte Carlo Methods in Atmospheric Optics* (Springer, Berlin, 1980).
[8]B. C. Wilson and G. Adam, "A Monte Carlo model for the absorption and flux distributions of light in tissue," Med. Phys. **10**, 824–830 (1983).
[9]S. A. Prahl, M. Keijzer, S. L. Jacques, and A. J. Welch, "A Monte Carlo model of light propagation in tissue," Proc. SPIE IS **5**, 102–111 (1989).
[10]L. Wang, S. L. Jacques, and L. Zheng, "MCML-Monte Carlo modeling of light transport in multi-layered tissues," Comput. Methods Programs Biomed. **47**, 131–146 (1995).
[11]Z. Song, K. Dong, X. H. Hu, and J. Q. Lu, "Monte Carlo simulation of converging laser beams propagating in biological materials," Appl. Opt. **38**, 2944–2949 (1999).
[12]J. Q. Lu, X. H. Hu, and K. Dong, "Modeling of the rough-interface effect on a converging light beam propagating in a skin tissue phantom," Appl. Opt. **39**, 5890–5897 (2000).
[13]H. Xu, T. J. Farrell, and M. S. Patterson, "Investigation of light propagation models to determine the optical properties of tissue from interstitial frequency domain fluence measurements," J. Biomed. Opt. **11**, 041104 (2006).
[14]C. Chen, J. Q. Lu, K. Li, S. Zhao, R. S. Brock, and X. H. Hu, "Numerical study of reflectance imaging using a parallel Monte Carlo method," Med. Phys. **34**, 2939–2948 (2007).
[15]N. Joshi, C. Donner, and H. W. Jensen, "Noninvasive measurement of scattering anisotropy in turbid materials by nonnormal incident illumination," Opt. Lett. **31**, 936–938 (2006).
[16]R. A. J. Groenhuis, H. A. Ferwerda, and J. J. Ten Bosch, "Scattering and absorption of turbid materials determined from reflection measurements. 1: Theory," Appl. Opt. **22**, 2456–2462 (1983).
[17]M. Keijzer, W. M. Star, and P. R. M. Storchi, "Optical diffusion in layered media," Appl. Opt. **27**, 1820–1824 (1988).
[18]M. S. Patterson, B. Chance, and B. C. Wilson, "Time resolved reflectance and transmittance for the noninvasive measurement of tissue optical properties," Appl. Opt. **28**, 2331–2336 (1989).
[19]T. J. Farrell, M. S. Patterson, and B. Wilson, "A diffusion theory model of spatially resolved, steady-state diffuse reflectance for the noninvasive determination of tissue optical properties *in vivo*," Med. Phys. **19**, 879–888 (1992).
[20]R. C. Haskell, L. O. Svaasand, T.-T. Tsay, T.-C. Feng, M. S. McAdams, and B. J. Tromberg, "Boundary conditions for the diffusion equation in radiative transfer," J. Opt. Soc. Am. A **11**, 2727–2741 (1994).
[21]A. H. Hielscher, S. L. Jacques, L. Wang, and F. K. Tittel, "The influence of boundary conditions on the accuracy of diffusion theory in time-resolved reflectance spectroscopy of biological tissues," Phys. Med. Biol. **40**, 1957–1975 (1995).
[22]A. Kienle and M. S. Patterson, "Improved solutions of the steady-state and the time-resolved diffusion equations for reflectance from a semi-infinite turbid medium," J. Opt. Soc. Am. A **14**, 246–254 (1997).
[23]G. W. Faris, "Diffusion equation boundary conditions for the interface between turbid media: A comment," J. Opt. Soc. Am. A **19**, 519–520 (2002).
[24]A. Ishimaru, *Wave Propagation and Scattering in Random Media* (Academic, New York, 1978).
[25]K. M. Case and P. F. Zweifel, *Linear Transport Theory* (Addison-Wesley, Reading, MA, 1967).
[26]C. Chen, J. Q. Lu, H. Ding, K. M. Jacobs, Y. Du, and X. H. Hu, "A primary method for determination of optical parameters of turbid samples and application to intralipid between 550 and 1630 nm," Opt. Express **14**, 7420–7435 (2006).
[27]L. Wang and S. L. Jacques, "Hybrid model of Monte Carlo simulation and diffusion theory for light reflectance by turbid media," J. Opt. Soc. Am. A **10**, 1746–1752 (1993).
[28]Y. Yamada, Y. Hasegawa, and Y. Yamashita, "Simulation of fan-beam-type optical computed-tomography imaging of strongly scattering and weakly absorbing media," Appl. Opt. **32**, 4808–4814 (1993).
[29]G. Alexandrakis, T. J. Farrell, and M. S. Patterson, "Monte Carlo diffusion hybrid model for photon migration in a two-layer turbid medium in the frequency domain," Appl. Opt. **39**, 2235–2244 (2000).
[30]G. Yoon, S. A. Prahl, and A. J. Welch, "Accuracies of the diffusion approximation and its similarity relations for laser irradiated biological media," Appl. Opt. **28**, 2250–2255 (1989).